ACS OMEGA

Open Access

http://pubs.acs.org/journal/acsodf

Article

Computational Insight into the Physical Properties of Bulk MP (M = Li, Na, K) for Energy Applications

Hafiza Sumaira Waheed, Mazia Asghar,* Hamid Ullah,* Muhammad Yaseen, Asad Ali, Akram Ibrahim, Amel Laref, and Ramesh Sharma

Cite This: *ACS Omega* 2024, 9, 22831−22838

Read Online

ACCESS | Metrics & More | Article Recommendations

ABSTRACT: In this study, we applied density functional theory to compute the electronic, optical, and thermal properties of MP (M = Li, Na, K). We find that the materials under consideration are stable, owing to the lack of negative frequencies in the phonon spectra. LiP exhibits an indirect band gap of 1.43 eV. NaP and KP have direct band gaps of 1.67 and 1.76 eV, respectively. The family of these composites shows strong absorption, observed by their very sharp absorption edges and confirmed by their direct transition from the valence to conduction band. They exhibit strong absorption below 4.0 eV in the optical spectra, which could serve in a solar cell device. The thermal calculations show high zT values of 0.74, 0.78, and 0.64 at 300 K for LiP, NaP, and KP, respectively. Thus, our results could be promising for electronic and thermal devices.

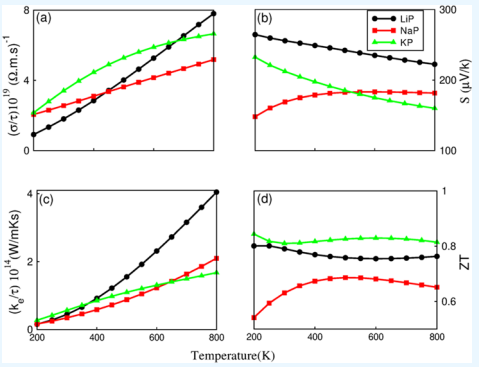

1. INTRODUCTION

Now, the world is overlooking the resources of fossil energy, and an alarming situation has been created due to inadequate fossil energy resources. The upcoming energy crisis makes scientists ponder developing environmentally friendly and renewable energy resources, as we know that solar energy is a renowned, vast, and copious source of energy.[1]

MP (M = Li, Na, K) have become a hot cake for research in recent years because of their use in solar cells, light emitting diode (LEDs),[2−4] photodetectors,[5−7] and lasers.[8−10] MP (M = Li, Na, K) have gained attention because of their high thermal conductivity and wide energy band gaps. Additionally, their direct band gap nature makes them more suitable for solar applications due to no energy loss.

It is a fact that low-band-gap materials like PbTe and Bi_2Te_3 are considered best for thermoelectric generators, and they are highly significant.[11] To understand the importance of materials in the application of renewable devices, a complete description of their properties is very crucial. The absorption coefficient, reflectivity, dielectric constants, and optical properties of PbTe and Bi_2Te_3 were computed using first-principles calculations by employing mBJ potentials.[12] LiP, NaP, and KP may cause surface oxidation or deterioration when they react with airborne moisture and oxygen. The reactivity of the sample may make handling, storing, and characterizing it more difficult. At high temperatures, a few phosphides, such as LiP, NaP, and KP, show poor thermal stability. This may reduce the variety of experimental conditions for studying the samples. Notwithstanding these difficulties, experimental research on these materials is crucial to expanding our knowledge of their basic characteristics and investigating their possible uses in a range of industries.

These alkali metals offer great promise for resolving the issues associated with the green energy crisis because of their unique characteristics in a range of renewable energy technologies. They can absorb a wider spectrum of sunlight, including visible and infrared light, since they have tunable direct band gaps in a visible region. Higher solar energy conversion efficiency may result from this characteristic. They may also be able to resolve the stability problems associated with conventional solar cell materials. Due to their better thermoelectric properties, these materials provide a way to utilize surplus heat from other sources or industrial operations by converting waste heat into power. These binary materials (MP) display potential in optoelectronics because of their special electronic structures, enabling effective heat-to-electricity conversion.

Although Li, Na, and K are all alkali metals, they differ considerably in mass and size. Because of this variance, the author may look into how the mass and size of the alkali metal impact the material's characteristics. Understanding how

Received: February 4, 2024
Revised: April 13, 2024
Accepted: April 17, 2024
Published: May 15, 2024

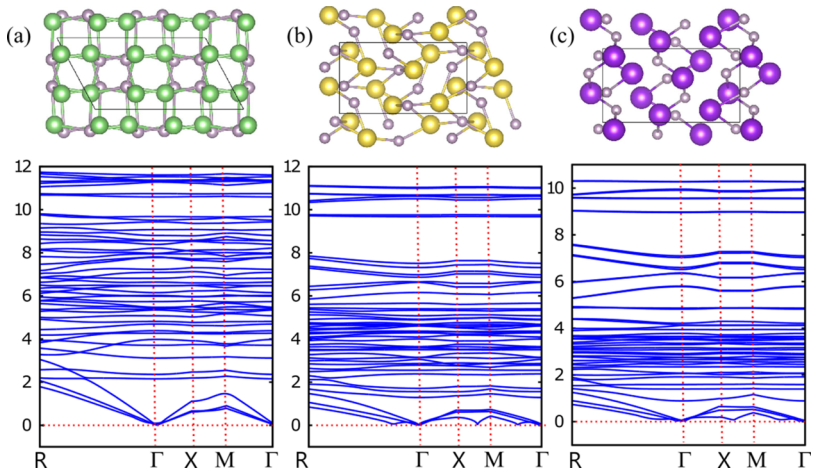

Figure 1. Relax structure geometry and the corresponding phonon spectra of (a) LiP, (b) NaP, and (c) KP.

Table 1. Calculated Lattice Constant (a_0), Unit Cell Volume (V_0), Bulk Modulus (B_0), Derivative of Bulk Modulus (B_p), and the Ground-State Energy (E_0) of MP (M = Li, Na, K)

compounds	a_0 (Bohr)	experimental (Å)	V_0 (au^3)	B (GPa)	B_P	E_0 (Ry)
LiP	a = 10.74	a = 5.5	1659.02	61.96	5.00	−5584.40
	b = 9.54	b = 4.9				
	c = 19.67	c = 10.1[24]				
NaP	a = 10.88	a = 6.03	2305.41	44.70	5.00	−8057.60
	b = 11.64	b = 5.64				
	c = 21.06	c = 10.14[25]				
KP	a = 11.53	a = 6.5	3004.30	33.92	5.00	−15,086.16
	b = 12.50	b = 6.01				
	c = 21.06	c = 11.28[25]				

atomic mass and radius variations affect the electronic structure, stability, and reactivity may be gained by density functional theory (DFT) calculations. They can absorb a wider spectrum of sunlight, including visible and infrared light, since they have tunable direct band gaps in a visible region. Additionally, because of the relative abundance of experimental data for molecules containing Li, Na, and K, theoretical models derived from DFT calculations may be validated and refined more easily.

Though a few works are available on the optical and electronic properties of MP (M = Li, Na, K), an organized theoretical study of the mentioned phosphides crucial for application purposes is missing in the literature. In the present study, we use first-principles calculations to investigate the optoelectronic and thermoelectric properties of MP (M = Li, Na, K). Our proposed materials are dynamically stable owing to non-negative vibrations in phonon spectra. Our calculated results show an indirect band gap of 1.43 eV for LiP. Interestingly, direct band gaps of 1.67 and 1.76 eV were observed for NaP and KP, correspondingly. The family of these compounds shows strong absorption in the visible region. These materials exhibit robust optical absorption in their optical absorption spectra beneath 4.0 eV, which could be capable of solar energy applications. The LiP, NaP, and KP possess high ZTs of 0.74, 0.78, and 0.64 at 300 K, respectively. Thus, our results could be promising for applications related to renewable energy devices.

2. METHODOLOGY

Based on the FP-LAPW technique, the WIEN2k code is an implementation of the DFT framework for the theoretical analysis of material characteristics of MP (M = Li, Na, K).[13,14] First, the generalized gradient approach (PBEsol-GGA) was used to optimize the structural parameters and obtain the optimal lattice parameters.[15] We then used the modified Becke−Johnson (mBJ) approach to ensure accurate band gap estimates because we observed that GGA has an impulse to underestimate the band gap value.[16] A spherical harmonic structure is expected for the ultimate electronic structure within the muffin-tin sphere, and a plane wave-like development is observed in the interstitial space. We first determined the Gaussian parameter G_{max} = 12 by multiplying the muffin-radius and wave vector ($R_{MT} \times K_{max}$ = 8). Then, we applied an angular momentum value of l_{max} = 10 in the reciprocal lattice to fine-tune the initial geometry. The Brillouin zone was integrated using a k-mesh with 2000 k-points, or a 12 × 12 × 12 grid, to guarantee precision.[16] It is assumed that the charge convergence is 0.01 mRy. Furthermore, the convergent energy and the enhanced electrical structures through mBJ have been taken into consideration in the computation of the transport characteristics utilizing the BoltzTraP code,[17] which is determined by the conventional Boltzmann transport theory.[18]

3. RESULTS AND DISCUSSION

3.1. Structural Properties. We relaxed the structure of MP (M = Li, Na, K), the LiP exhibits a monoclinic geometry with the space group $P2_1/C$,[14] while NaP and KP possess orthorhombic structures with the space group $P2_12_12_1$,[19] as

https://doi.org/10.1021/acsomega.4c01116
ACS Omega 2024, 9, 22831−22838

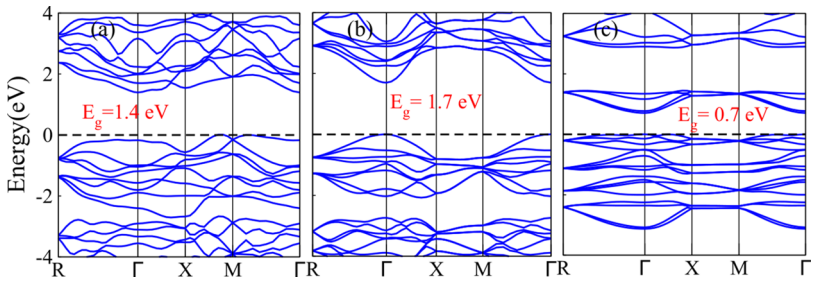

Figure 2. Calculated band structures of (a) LiP, (b) NaP, and (c) KP.

shown in Figure 1. We have used PBEsol-GGA for optimization of these compounds by using the Birch–Murnaghan equation of states to determine the lattice parameter at the ground state. The lattice constant (a_0) at the ground state and the bulk modulus are calculated by computing the volume optimization method in Table 1. From Table 1, it can be seen that the a_0 of the studied materials improves as we go from Li to K due to the increasing trend in the ionic radii as r_{Li} (1.45 Å) < r_{Na} (1.80 Å) < r_K (2.20 Å). Thus, the increasing trend in the ionic radii of group-III elements enhances the interatomic spacing, resulting an increase in the lattice constant.[19−21] In order to calculate the resistance of material resistance against the external pressure, the bulk modulus is also calculated for MP (M = Li, Na, K). We find a decreasing trend as we move from Li to K, as tabulated in Table 1. The decreasing trend in the bulk modulus (from Li to K) exhibits that MP (M = Li, Na, K) are compressible because of the increasing volume of the unit cell (due to the lattice constant increase). Therefore, an inverse relation exists between the lattice constant and the bulk modulus, $B \propto \frac{1}{a_0}$,[22,23] where the unit cell volume is represented by V_0.

To check the stability of MP (M = Li, Na, K), we have computed the phonon spectra by employing a finite-displacement approach using the Phonopy code.[26] The phonon spectra have been computed beside the great symmetry R–Γ–X–M–Γ commands of the Brillouin zone, as depicted in Figure 1. The absence of imaginary frequency in computed spectra confirms the stable nature of MP (M = Li, Na, K), like SnSSe[27] and others.[23,28]

3.2. Electronic Properties. After confirming the stable nature of MP (M = Li, Na, K), we further calculated the electronic properties with the mBJ method. The band gap for LiP is estimated to be 1.43 eV, showing its indirect band gap nature, as shown in Figure 2. From Figure 2, it is clearly understood that the extreme of the valence band (VBM) stands among M–Γ points and the lowest of the conduction band (CBM) is at the Γ point, revealing the indirect band gap nature of LiP. Interestingly, NaP and KP possess direct band gaps of 1.67 and 1.76 eV, respectively, as shown in Figure 2 and Table 2. From Figure 2, one can see that the VBM and CBM lie at a similar symmetry point (Γ), confirming the direct band gaps of NaP and KP. Our calculated band gap is comparable with the values of Li_2Se, Na_2Se, and K_2Se, i.e., 2.80, 2.01, and 2.2 eV, respectively.

To obtain a more detailed understanding of the electron contribution inside the band structure from the various states, the total/partial density of states (T/PDOS) of MP (M = Li, Na, K) is computed, also shown in Figure 3. The Li/Na/K p-states are dominant and have negligibly less contribution from

Table 2. Calculated Band Gap (E_g) and Optical Parameters at 0 eV Energy for MP (M = Li, Na, K) Using the mBJ Potential

	E_g (eV)				
compounds	this work	others	ε_1 (0)	n (0)	R (0)
LiP	1.43	AlAs = 1.42[29]	8.6	2.90	0.25
NaP	1.67	SiP = 1.69[30]	7.3	2.64	0.21
KP	1.76	K_2Te = 1.42[31]	5.8	2.45	0.16

s-states of corresponding atoms at the lower valence band of the TDOS. Thus, the p-states of Li, Na, and K mostly contribute to the DOS. Similarly, the p-states of Li, Na, and K mainly contribute to the conduction band.

3.3. Optical Properties. Furthermore, we have estimated the optical properties of MP (M = Li, Na, K) for technological applications. We have studied their optical properties to find their suitability in photovoltaic cells. The dielectric function is determined to observe the material's response to the frequency or the electric field of the incident photon. The dielectric function describes the limit of propagation of an electromagnetic wave in terms of the complex function of the angular frequency (ω) of the external electric charges. In order to compute all optical properties inspected in MP (M = Li, Na, K), the complex dielectric function $\varepsilon(\omega)$ is calculated. We have estimated the optical properties of MP (M = Li, Na, K) in terms of reflectivity, refraction, and absorption. We used the Kramer–Kroning transformation to calculate the real dielectric constants from the imaginary part of dielectric constants from eqs 1 and 2.[32]

$$\varepsilon_1(\omega) = 1 + \frac{2}{\pi} P \int_0^\infty \frac{\omega' \varepsilon 2(\omega')}{\omega' 2 - \omega' 2} \mathrm{d}\omega' \quad (1)$$

$$\varepsilon_2(\omega) = \frac{e^2 \dot{h}}{\pi m^2 \omega^2} \sum_{v,c} \int_{BZ}^\infty |Mcv(k)|2\delta[\omega cv(k) - \omega] \mathrm{d}^3 k \quad (2)$$

$\varepsilon_1(\omega)$ is the real part of the dielectric constant that explains how much the materials are polarized at the plasmonic resonance frequency and their variations with photon energy.

We have used $\varepsilon(\omega)$, which contains two parts, the real part ($\epsilon_1(\omega)$) and the imaginary ($\epsilon_2(\omega)$) part, as shown in Figure 4. $\epsilon_1(\omega)$ shows the ability of a material to store energy and has a direct relation with the refractive index of a system.[33] Furthermore, $\epsilon_1(\omega)$ exhibits electronic polarizability, which can be defined as shifting the positive and negative electric charges in the reverse directions.[33] Moreover, the behavior, capability of absorbing light, and energy gain for the photovoltaic materials[34] can be evaluated from the $\epsilon_2(\omega)$ part of $\varepsilon(\omega)$. Also, $\epsilon_2(\omega)$ presents the absorption of light,

https://doi.org/10.1021/acsomega.4c01116
ACS Omega 2024, 9, 22831−22838

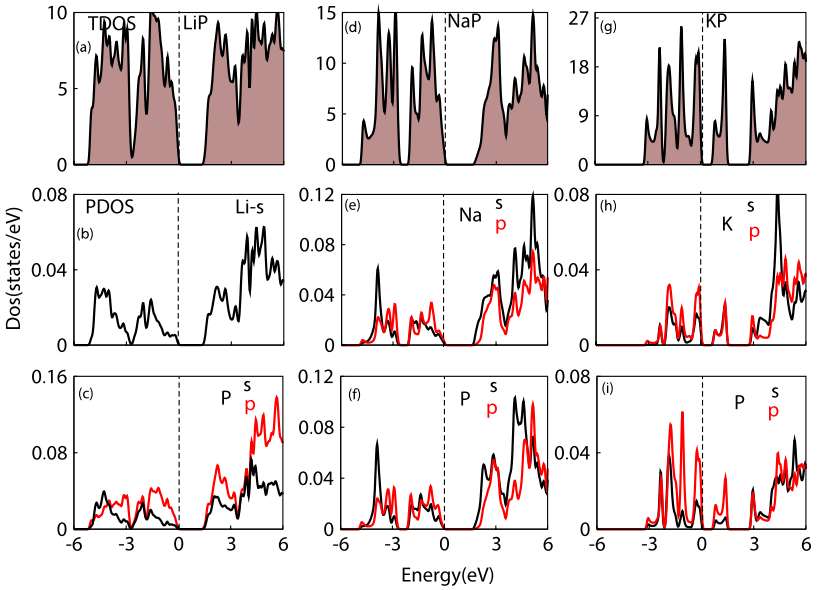

Figure 3. Total and partial density of states of (a–c) LiP, (d–f) NaP, and (g–i) KP.

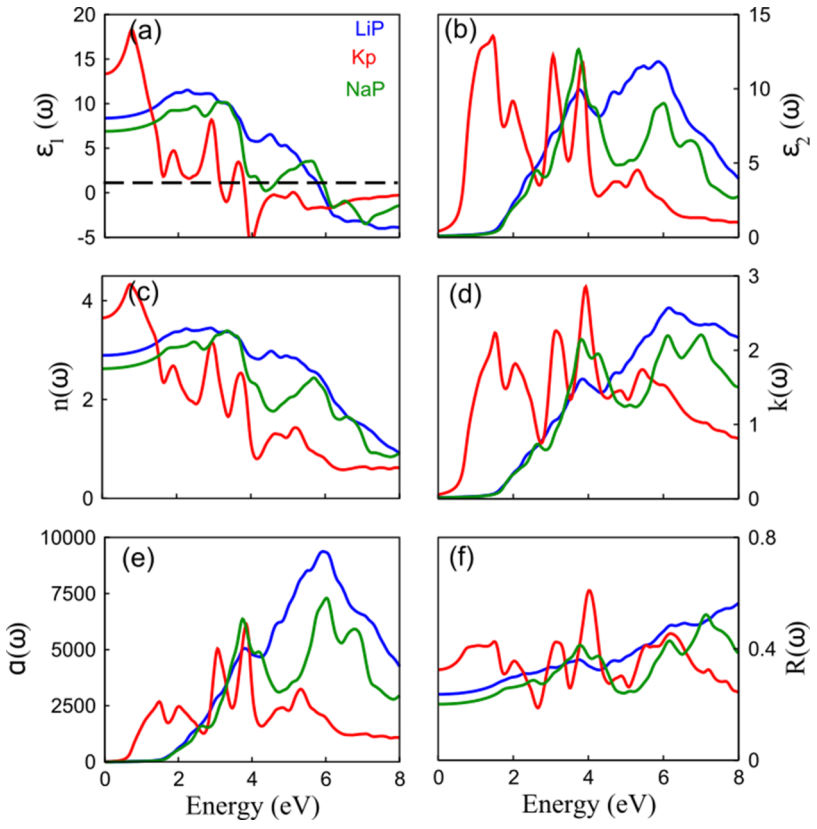

Figure 4. Calculated (a) real part ($\epsilon_1(\omega)$) and (b) imaginary part ($\epsilon_2(\omega)$) of the dielectric, (c) refractive index ($n(\omega)$), (d) extinction coefficient ($k(\omega)$), (e) absorption coefficient ($\alpha(\omega)$), and (f) reflectivity ($R(\omega)$) of MP (M = Li, Na, K).

which is the shift of electrons from the ground state to the excited state. From Figure 4, an increasing trend in $\epsilon_1(\omega)$ can be seen in the zero-frequency limit for MP (M = Li, Na, K). In Figure 4, we can see that at 2.2, 3.3, and 3.6 eV energy, a steady variation occurs in $\epsilon_1(\omega)$ after the preliminary transition. The negative value of $\epsilon_1(\omega)$ in Figure 4(a) represents the electromagnetic wave reflectance for LiP, NaP, and KP. In the zero frequency, the larger $\epsilon_1(\omega)$ value suggests the high polarizability of the studied material, as shown in Figure 4(a). $\epsilon_1(\omega)$ is defined as the square of the refractive index (n).[33] Thus, the n value is estimated to be 2.90, 2.64, and 2.45 for LiP, NaP, and KP, respectively (see Figure 4). Our computed values of n are higher than those of tin sulfide (1.94),[35] tin selenide (1.98),[35] zinc sulfide (1.661),[36] and phosphorene (1.20),[37] though comparable to graphene (2.69)[38]

The high n values in the visible spectrum suggest an extensive variety of applications of MP (M = Li, Na, K). For instance, they can be used as substrates in advanced display

https://doi.org/10.1021/acsomega.4c01116
ACS Omega 2024, 9, 22831−22838

devices[39] and have the capability in photonics as antireflectors[40] and optical encapsulants with optimized refractive indices to boost the response of photovoltaic cells.[41] The imaginary part $\epsilon_2(\omega)$ of MP (M = Li, Na, K) exhibits strong absorption, which shows that these materials can better absorb light in the visible range to 3.4 eV, which could be capable of increasing the absorption of the solar energy spectrum.

Figure 4(c) shows the relation between the incident light in electronvolt and the refractive index ($n(\omega)$), whereas Figure 4(d) displays the relation between the incident light in electronvolt and the extinction coefficient ($k(\omega)$). The overall profiles of $k(\omega)$ and $n(\omega)$ of MP (M = Li, Na, K) are quite similar. Static $n(\omega)$ is estimated to be 2.90, 2.64, and 2.45 for LiP, NaP, and KP, respectively, and reached the peak values of 3.43, 3.38, and 3.58 at 2.78, 3.10, and 3.23 eV, respectively. Thereafter, a steady decrease is seen, tending to a constant value in the far UV region. The $k(\omega)$ values of 0.63 (NaP) and 0.82 (KP) exhibit two peaks at 2.74 and 2.24 eV, respectively. The second peak lies in the UV region, whereas for LiP, both peaks appear in the UV region. The resonance in the graph of $n(\omega)$ and $k(\omega)$ in the UV region leads toward the interband transition in MP (M = Li, Na, K). The width of the peak demonstrates the rate at which the photons are being absorbed in the specified range. To calculate the refractive index and the extinction coefficient, eqs 3 and 4 are as follows

$$n = \left\{ [(\epsilon_1^{\,2} + \epsilon_2^{\,2})^{1/2} + \epsilon_2]\frac{1}{2} \right\}^{1/2} \tag{3}$$

$$k = \left\{ [(\epsilon_1^{\,2} + \epsilon_2^{\,2})^{1/2} - \epsilon_2]\frac{1}{2} \right\}^{1/2} \tag{4}$$

where the real and imaginary parts of the complex dielectric function are represented by ϵ_1 and ϵ_2, respectively.

The low energy range (0.00−3.30 eV) in Figure 4 describes that the absorption coefficient ($\alpha(\omega)$) fits well with the $\epsilon_2(\omega)$ curves, which corresponds to the electronic transition, as presented in Figure 2. We have estimated the $\alpha(\omega)$ values to be 63 at 3.9 eV, 80 at 3.9 eV, and 87.5 at 3.57 eV for LiP, NaP, and KP, respectively, and then peaks proceed in the ultraviolet region. These outcomes illustrate the higher absorption in the UV region. In view of the above discussion, MP (M = Li, Na, K) could be a promising entity to the family of optoelectronic materials for applications in photovoltaic (PV), etc. Equation 5 describes the absorption coefficient α.

$$\alpha = \frac{2k(\omega)}{c} \tag{5}$$

In Figure 4, the reflectivity ($R(\omega)$) and energy loss function ($L(\omega)$) have been calculated and plotted as a function of energy. From Figure 4, we can see that from 0 to 3.0 eV (the low energy region), the values of reflectivity spectra $R(\omega)$ are significantly small, indicating that transition does not take place in the given spectrum. Therefore, the $R(\omega)$ value in the UV spectrum is higher in comparison with the visible spectrum; at 3.65 eV, the percentage of reflection is about 45%. Reflections of about 15% take place in the visible region. The behavior of MP (M = Li, Na, K) from the infrared (IR) to UV region marks it as a potential candidate for IR and UV region applications. From eq 6, we can calculate the reflectivity of a material.

$$R = \frac{(n-1)^2 + k^2}{(n+1)^2 + k^2} \tag{6}$$

The high absorption can be observed at the energy where the transition occurs. The electron gets excited in a medium when the photon obtains sufficient energy. In a solid medium, a fast-moving electron can bump in to other electrons, which results in the excitation of other electrons that de-excite and release energy. Consequently, the communal excitation occurs that can be specified by the energy loss spectrum, $L(\omega)$, and is related to the dielectric constant $\varepsilon(\omega)$. During the inter- and intraband transitions, $L(\omega)$ can be distinguished by the excitation of plasmons. The plasma resonance properties are exhibited by the peak value in $L(\omega)$, and the subsequent frequency is known as the plasma frequency. The electron may respond at the plasma frequency. Therefore, if incident light (photon) can not have an energy equal to plasma frequency, the electric field is able to screen effectively by plasma oscillation. From Figure 4, one can see that the highest peaks are at 11.0 and 12.0 eV, showing plasmon resonance.

3.4. Thermoelectric Properties. Our world is facing a great energy crisis economically and as well as environmentally.[42] Scientists are trying to overcome this deficiency by converting waste energy into electrical energy,[43−46] and this electrical energy has been used in potential applications like heating and cooling devices in electronics and spintronics.[5−8] We have calculated the thermoelectric properties of LiP, NaP, and KP using BoltzTrap software in WIEN2k.[47] We have also calculated the Seebeck coefficient (S), thermal conductivity (k), power factor (PF), and electrical conductivity (σ), and after that, we made the figure of merits (zT).

The following expressions have been used for calculations.

$$\sigma_{\alpha\beta}(\varepsilon) = \frac{1}{N}\sum_{i,k}\sigma_{\alpha\beta}(i,k)\frac{\delta(\varepsilon - \varepsilon_{i,k})}{\delta(\varepsilon)} \tag{7}$$

$$\sigma_{\alpha\beta}(i,k) = e^2\tau_{i,k}\vartheta_\alpha(i,k)\vartheta_\beta(i,k) \tag{8}$$

Here, the wave vector is k and the number of k-points is represented by N. τ is the time and the group velocity is symbolized by $\upsilon_\beta(i,k)$. Other values required for the calculation of thermoelectric are described as follows.

$$\sigma_{\alpha\beta}(\alpha,\mu) = \frac{1}{2}\int\sigma_{\alpha\beta}(\varepsilon)\left[-\frac{\partial f_0(T,\varepsilon,\mu)}{\partial\varepsilon}\right]\mathrm{d}\varepsilon \tag{9}$$

$$S_{\alpha\beta}(T,\mu) = \frac{1}{eT\Omega\sigma_{\alpha\beta(T,\mu)}}\int\sigma_{\alpha\beta}(\varepsilon)(\varepsilon\mu)\left[-\frac{\partial f_0(T,\varepsilon,\mu)}{\partial\varepsilon}\right]\mathrm{d}\varepsilon \tag{10}$$

Electrical conductivity is represented by α, unit cell volume is shown by Ω, β is the electron charge in the concentration of the carrier, and the Fermi Dirac distribution is represented by f_0. The output efficiency can be measured by the following equation.

$$\mathrm{zT}\left(\frac{\sigma S^2}{k}\right)\mathrm{T} \tag{11}$$

Here, we have electrical conductivity as α, S is the Seebeck coefficient, thermal conductivity is represented by K, and T is the temperature. σ and S increase with an increase in temperature and then start decreasing. In order to calculate

https://doi.org/10.1021/acsomega.4c01116
ACS Omega 2024, 9, 22831−22838

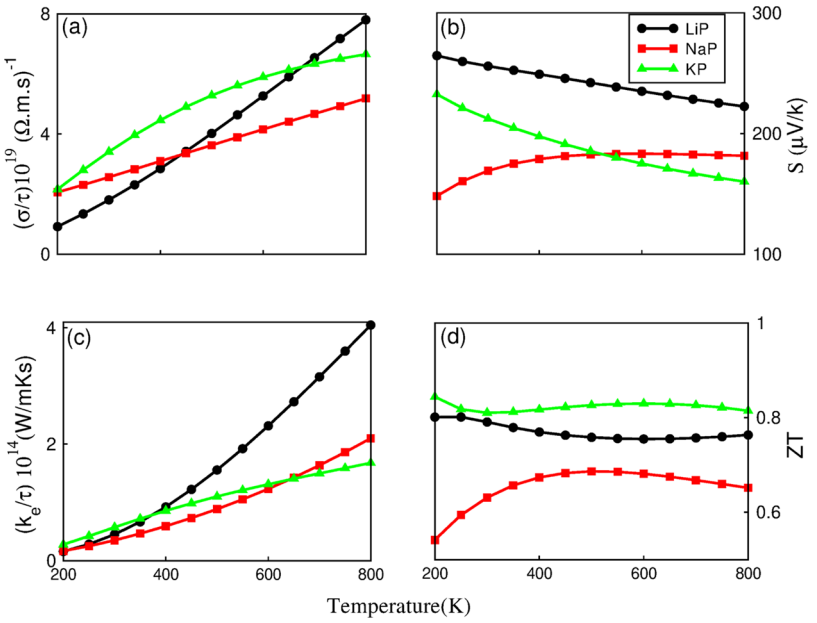

Figure 5. (a) Electrical conductivity (σ/τ), (b) Seebeck coefficient (S), (c) thermal conductivity (k/τ), and (d) figure of merit (ZT) for LiP, NaP, and KP.

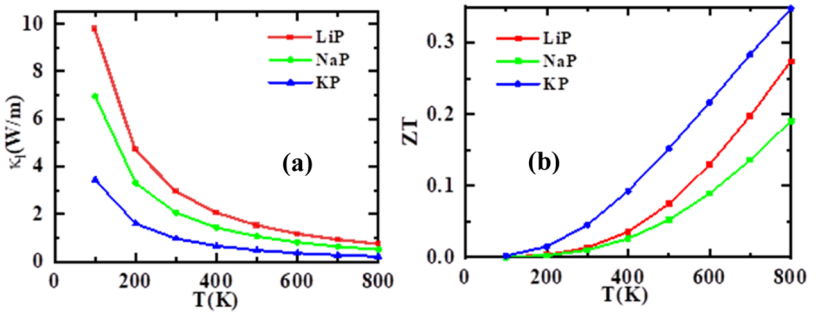

Figure 6. Computed (a) lattice thermal conductivity and (b) figure of merit for MP (M = Li, Na, K) at 300 K.

the electrical and thermal conductivity, the relaxation time (τ) can be used in traditional Boltzmann transport software. The default value of relaxation time is $\tau = 10^{-15}$. But, we set the relaxation time as $\tau = 10^{-14}$. Figure 5(a) represents the plot of electrical conductivity as a function of temperature (k), where the temperature ranges from 200 to 800 (k). We can observe that in Figure 5(a), LiP shows the maximum electrical conductivity, while NaP and KP show linear behavior. If we observe electrical conductivity at room temperature, then we can see that at 300 K, LiP shows 3×10^{18} $(\Omega\ \mathrm{ms})^{-1}$, NaP shows 1×10^{18} $(\Omega\ \mathrm{ms})^{-1}$, and KP shows 0.8×10^{18} $(\Omega\ \mathrm{ms})^{-1}$.[48] We will only consider the electronic component because of some limitation of the BoltzTraP code according to our observation.

Calculation of the Seebeck coefficient has been shown in Figure 5(b). In the Seebeck coefficient, we observe the magnitude of the induced value of volume. Here, NaP shows the maximum value of the Seebeck coefficient. At room temperature, the values of the Seebeck coefficient of LiP, NaP, and KP are 0.20, 0.24, and 0.22 μV/k, respectively.

Figure 5(c) shows the thermal conductivity of our compounds and exhibits that LiP shows the maximum thermal conductivity. We can also observe the thermal conductivity values of these compounds at room temperature, i.e., 0.5×10^{14} (W/m K s) for LiP, 0.2×10^{14} (W/m K s) for NaP, and 0.3×10^{14} (W/m K s) for KP.

Figure 5(d) shows that the thermal proficiency is explained with the figure of merit (ZT) data. MP (M = Li, Na, K) compounds do not show significant values of zT at 300 K, so the zT value can be enhanced using advanced theories. The thermal and electrical transport features of thermoelectric materials provide novel opportunities for thermoelectric performance enhancement.[49]

Using the mathematical formula $q = -k\frac{dq}{dx}$, Fourier's law defines the heat flow in a thermoelectric material. The temperature gradient is represented by the expression $\frac{dq}{dx}$, the coefficient of thermal conductivity is denoted by "k," and "q" stands for the rate of thermal energy flow per unit area over time. In semiconductors, phonons and electrons both affect the total thermal conductivity; in metals, however, the phonon contribution is small, less than 2%. This coupling has been included in the research of thermoelectric properties under examination, as the transport characteristics are greatly influenced by the interaction between electrons and phonons. Two different methods have been used to analyze thermal conductivity: the electron- and the phonon-based methods, which are represented by the formula $\kappa t = \kappa e + \kappa l$. The contribution from electron vibration is denoted by κe in this

https://doi.org/10.1021/acsomega.4c01116
ACS Omega 2024, 9, 22831−22838

formula, while the thermal conductivity related to phonon vibration is represented by κl. The computed thermal conductivities attributed to the phononic (κl) processes across the temperature range of 0−800 K are shown in Figure 6(a), which illustrates this connection. The graphs for κl and total or overall conductivity, both of which drop with increasing temperature, indicate the thermal conductivities.

4. SUMMARY

In summary, we have calculated the optoelectronic and thermal properties of MP (M = Li, Na, K) using first-principles calculations. First, we investigated the basic structural properties of MP (M = Li, Na, K) (LiP, NaP, and KP). LiP possesses monoclinic geometry, while NaP and KP exhibit orthorhombic structures. The phonon spectra showed that the system under consideration is dynamically stable due to no imaginary frequencies in the spectra. Our result indicates the indirect band gap for LiP, that is, 1.43 eV. Interestingly, both NaP and KP possess direct band gaps of 1.67 and 1.76 eV, respectively. The family of these compounds shows strong absorption, and the reflectivity is lower than 15% in the visible spectrum region. Hence, in the visible region, they absorb most of the incident light and could show promising results in solar cells. From the thermal calculations, we find high zT values of 0.74, 0.78, and 0.64 at 300 K for LiP, NaP, and KP, respectively. Hence, our results could be worthwhile for future experimental work to explore these compounds for applications related to renewable energy devices.

AUTHOR INFORMATION

Corresponding Authors

Hamid Ullah − *Department of Physics, Riphah International University, Islamabad, Lahore 54000, Pakistan*; Email: hamid.uou@gmail.com

Mazia Asghar − *Department of Physics, Riphah International University, Islamabad, Lahore 54000, Pakistan*; Email: maziaasghar915@gmail.com

Authors

Hafiza Sumaira Waheed − *Department of Physics, Riphah International University, Islamabad, Lahore 54000, Pakistan*

Muhammad Yaseen − *Department of Computer Science, Riphah International University, Islamabad, Lahore 54000, Pakistan*

Asad Ali − *Multiscale Materials Modeling Laboratory, Department of Physics, University of Ulsan, Ulsan 44610, Republic of Korea*

Akram Ibrahim − *Department of Physics, College of Science, King Khalid University, Abha 61413, Kingdom of Saudi Arabia*

Amel Laref − *Department of Physics and Astronomy, College of Science, King Saud University, Riyadh 11451, King Saudi Arabia*

Ramesh Sharma − *Department of Applied Science, Feroze Gandhi Institute of Engineering and Technology, Raebareli 229001 Uttarpradesh, India*

Complete contact information is available at: https://pubs.acs.org/10.1021/acsomega.4c01116

Author Contributions

H.S.W. wrote the initial draft and performed the calculations, M.A. edited the draft and performed formal analysis, H.U. did supervision and conceptualization, M.Y. performed formal analysis, A.A. performed phonon calculations, A.I. and A.L. performed formal analysis and edited the manuscript, and R.S. performed the lattice thermal conductivity calculations.

Notes

The authors declare no competing financial interest.

ACKNOWLEDGMENTS

The authors extend their appreciation to the Deanship of Scientific Research at King Khalid University for funding this work through a large group Research Project under grant number RGP2/450/44.

REFERENCES

(1) Fox, M. A.; Dulay, M. T. Heterogeneous Photocatalysis. *Chem. Rev.* **1993**, *93* (1), 341−357.

(2) Yantara, N.; Bhaumik, S.; Yan, F.; Sabba, D.; Dewi, H. A.; Mathews, N.; Boix, P. P.; Demir, H. V.; Mhaisalkar, S. Inorganic Halide Perovskites for Efficient Light-Emitting Diodes. *J. Phys. Chem. Lett.* **2015**, *6* (21), 4360−4364.

(3) Wong, A. B.; Lai, M.; Eaton, S. W.; Yu, Y.; Lin, E.; Dou, L.; Fu, A.; Yang, P. Growth and Anion Exchange Conversion of CH3NH3PbX3 Nanorod Arrays for Light-Emitting Diodes. *Nano Lett.* **2015**, *15* (8), 5519−5524.

(4) Tan, Z.-K.; Moghaddam, R. S.; Lai, M. L.; Docampo, P.; Higler, R.; Deschler, F.; Price, M.; Sadhanala, A.; Pazos, L. M.; Credgington, D.; Hanusch, F.; Bein, T.; Snaith, H. J.; Friend, R. H. Bright Light-Emitting Diodes Based on Organometal Halide Perovskite. *Nat. Nanotechnol.* **2014**, *9* (9), 687−692.

(5) Dou, L.; Yang, Y.; Micheal; You, J.; Hong, Z.; Chang, W.-H.; Li, G.; Yang, Y. Solution-Processed Hybrid Perovskite Photodetectors with High Detectivity. *Nat. Commun.* **2014**, *5* (1), No. 5404.

(6) Li, X.; Yu, D.; Chen, J.; Wang, Y.; Cao, F.; Wei, Y.; Wu, Y.; Wang, L.; Zhu, Y.; Sun, Z.; Ji, J.; Shen, Y.; Sun, H.; Zeng, H. Constructing Fast Carrier Tracks into Flexible Perovskite Photodetectors To Greatly Improve Responsivity. *ACS Nano* **2017**, *11* (2), 2015−2023.

(7) Bao, C.; Yang, J.; Bai, S.; Xu, W.; Yan, Z.; Xu, Q.; Liu, J.; Zhang, W.; Gao, F. High Performance and Stable All-Inorganic Metal Halide Perovskite-Based Photodetectors for Optical Communication Applications. *Adv. Mater.* **2018**, *30* (38), No. 1803422.

(8) Kim, H.-S.; Im, S. H.; Park, N.-G. Organolead Halide Perovskite: New Horizons in Solar Cell Research. *J. Phys. Chem. C* **2014**, *118* (11), 5615−5625.

(9) Green, M. A.; Ho-Baillie, A.; Snaith, H. J. The Emergence of Perovskite Solar Cells. *Nat. Photonics* **2014**, *8* (7), 506−514.

(10) Grätzel, M. The Light and Shade of Perovskite Solar Cells. *Nat. Mater.* **2014**, *13* (9), 838−842.

(11) Noor, N. A.; Iqbal, M. W.; Zelai, T.; Mahmood, A.; Shaikh, H. M.; Ramay, S. M.; Al-Masry, W. Analysis of Direct Band Gap A2ScInI6 (A = Rb, Cs) Double Perovskite Halides Using DFT Approach for Renewable Energy Devices. *J. Mater. Res. Technol.* **2021**, *13*, 2491−2500.

(12) Tran, F.; Blaha, P. Accurate Band Gaps of Semiconductors and Insulators with a Semilocal Exchange-Correlation Potential. *Phys. Rev. Lett.* **2009**, *102* (22), No. 226401.

(13) Blaha, P.; Schwarz, K.; Madsen, G. K.; Kvasnicka, D.; Luitz, J. *WIEN2k: An Augmented Plane Wave + Local Orbitals Program for Calculating Crystal Properties*; Technische Universität, 2001; Vol. *60*.

(14) Blaha, P.; Schwarz, K.; Madsen, G. K. H.; Kvasnicka, D.; Luitz, J.; Laskowsk, R.; Tran, F.; Marks, L.; Marks, L. *WIEN2k: An Augmented Plane Wave Plus Local Orbitals Program for Calculating Crystal Properties*; Techn. Universitat, 2019.

(15) Baerends, E. J.; Gritsenko, O. V. Away from Generalized Gradient Approximation: Orbital-Dependent Exchange-Correlation Functionals. *J. Chem. Phys.* **2005**, *123* (6), No. 062202.

(16) Koller, D.; Tran, F.; Blaha, P. Improving the Modified Becke-Johnson Exchange Potential. *Phys. Rev. B* **2012**, *85*. DOI: 10.1103/PhysRevB.85.155109.
(17) Madsen, G. K. H.; Singh, D. J. BoltzTraP. A Code for Calculating Band-Structure Dependent Quantities. *Comput. Phys. Commun.* **2006**, *175* (1), 67−71.
(18) Li, W.; Carrete, J.; Katcho, N. A.; Mingo, N. ShengBTE: A Solver of the Boltzmann Transport Equation for Phonons. *Comput. Phys. Commun.* **2014**, *185* (6), 1747−1758.
(19) Ali, R.; Mohammad, S.; Ullah, H.; Khan, S. A.; Uddin, H.; Khan, M.; Khan, N. U. The Structural, Electronic and Optical Response of IIA−VIA Compounds through the Modified Becke−Johnson Potential. *Phys. B* **2013**, *410*, 93−98.
(20) Pressure Effects on Structure and Optical Properties in Cesium Lead Bromide Perovskite Nanocrystals|Journal of the American Chemical Society https://pubs.acs.org/doi/abs/10.1021/jacs.7b05260 (accessed July 6, 2022).
(21) Ge, L.; Zhang, M.; Wang, R.; Li, N.; Zhang, L.; Liu, S.; Jiao, T. Fabrication of CS/GA/RGO/Pd Composite Hydrogels for Highly Efficient Catalytic Reduction of Organic Pollutants. *RSC Adv.* **2020**, *10* (26), 15091−15097.
(22) Hassan, M.; Arshad, I.; Mahmood, Q. Computational Study of Electronic, Optical and Thermoelectric Properties of X3PbO (X= Ca, Sr, Ba) Anti-Perovskites. *Semicond. Sci. Technol.* **2017**, *32* (11), No. 115002.
(23) Aslam, F.; Ullah, H.; Hassan, M. First Principle Study of Band Gap Tuning in Cs2InSbX6 (X= Cl, Br, I) for Optoelectronic and Thermoelectric Applications. *Phys. Scr.* **2022**, *97* (4), No. 045801.
(24) Langer, K.; Juza, R. Über das Lithiummonophosphid. *Naturwissenschaften* **1967**, *54* (9), 225.
(25) Georg, H.; Schnering, V.; Hönle, W. Zur Chemie und Strukturchemie der Phosphide und Polyphosphide. 20. Darstellung, Struktur und Eigenschaften der Alkalimetallmonophosphide NaP und KP. *Z. Anorg. Allg. Chem.* **1979**, *456* (1), 194−206.
(26) Togo, A.; Tanaka, I. First Principles Phonon Calculations in Materials Science. *Scr. Mater.* **2015**, *108*, 1−5.
(27) Alam, M.; Waheed, H. S.; Ullah, H.; Iqbal, M. W.; Shin, Y.-H.; Iqbal Khan, M. J.; Elsaeedy, H. I.; Neffati, R. Optoelectronics Properties of Janus SnSSe Monolayer for Solar Cells Applications. *Phys. B* **2022**, *625*, No. 413487.
(28) Aslam, F.; Ullah, H.; Hassan, M. Theoretical Investigation of Cs2InBiX6 (X= Cl, Br, I) Double Perovskite Halides Using First-Principle Calculations. *Mater. Sci. Eng., B* **2021**, *274*, No. 115456.
(29) Owolabi, J. A.; Onimisi, M. Y.; Abdu, S. G.; Olowomofe, G. O. Determination of Band Structure of Gallium-Arsenide and Aluminium-Arsenide Using Density Functional Theory. *Comput. Chem.* **2016**, *04* (03), 73−82.
(30) Zhang, S.; Guo, S.; Huang, Y.; Zhu, Z.; Cai, B.; Xie, M.; Zhou, W.; Zeng, H. Two-Dimensional SiP: An Unexplored Direct Band-Gap Semiconductor. *2D Mater.* **2017**, *4* (1), No. 015030.
(31) Alay-e-Abbas, S. M.; Shaukat, A. FP-LAPW Calculations of Structural, Electronic, and Optical Properties of Alkali Metal Tellurides: M2Te [M: Li, Na, K and Rb]. *J. Mater. Sci.* **2011**, *46* (4), 1027−1037.
(32) Rehman, S. U.; Butt, F. K.; Haq, B. U.; AlFaify, S.; Khan, W. S.; Li, C. Exploring Novel Phase of Tin Sulfide for Photon/Energy Harvesting Materials. *Sol. Energy* **2018**, *169*, 648−657.
(33) Berdiyorov, G. R.; Kachmar, A.; El-Mellouhi, F.; Carignano, M. A.; El-Amine Madjet, M. Role of Cations on the Electronic Transport and Optical Properties of Lead-Iodide Perovskites. *J. Phys. Chem. C* **2016**, *120* (30), 16259−16270.
(34) Lashgari, H.; Boochani, A.; Shekaari, A.; Solaymani, S.; Sartipi, E.; Mendi, R. T. Electronic and Optical Properties of 2D Graphene-like ZnS: DFT Calculations. *Appl. Surf. Sci.* **2016**, *369*, 76−81.
(35) Huang, Y.; Chen, X.; Zhou, D.; Liu, H.; Wang, C.; Du, J.; Ning, L.; Wang, S. Stabilities, Electronic and Optical Properties of SnSe2(1−x)S2x Alloys: A First-Principles Study. *J. Phys. Chem. C* **2016**, *120* (10), 5839−5847.
(36) Liu, Q.; Luo, D.; Zhang, X.; Li, S.; Tian, Z. Refractive Index and Absorption Coefficient of Blue Phase Liquid Crystal in Terahertz Band. *Liq. Cryst.* **2017**, *44* (2), 348−354.
(37) Weber, J. W.; Calado, V. E.; van de Sanden, M. C. M. Optical Constants of Graphene Measured by Spectroscopic Ellipsometry. *Appl. Phys. Lett.* **2010**, *97* (9), No. 091904.
(38) Nakamura, T.; Fujii, H.; Juni, N.; Tsutsumi, N. Enhanced Coupling of Light from Organic Electroluminescent Device Using Diffusive Particle Dispersed High Refractive Index Resin Substrate. *Opt. Rev.* **2006**, *13*, 104−110.
(39) Bouhafs, D.; Moussi, A.; Chikouche, A.; Ruiz, J. M. Design and Simulation of Antireflection Coating Systems for Optoelectronic Devices: Application to Silicon Solar Cells. *Sol. Energy Mater. Sol. Cells* **1998**, *52* (1), 79−93.
(40) Ma, M.; Mont, F. W.; Poxson, D. J.; Cho, J.; Schubert, E. F.; Welser, R. E.; Sood, A. K. Enhancement of Photovoltaic Cell Response Due to High-Refractive-Index Encapsulants. *J. Appl. Phys.* **2010**, *108* (4), No. 043102.
(41) Ren, K.; Sun, M.; Luo, Y.; Wang, S.; Yu, J.; Tang, W. First-Principle Study of Electronic and Optical Properties of Two-Dimensional Materials-Based Heterostructures Based on Transition Metal Dichalcogenides and Boron Phosphide. *Appl. Surf. Sci.* **2019**, *476*, 70−75.
(42) Allcott, H. Social Norms and Energy Conservation. *J. Public Econ.* **2011**, *95* (9), 1082−1095.
(43) Lu, Z.; Salamon, T. R.; Narayanan, S.; Bagnall, K. R.; Hanks, D. F.; Antao, D. S.; Barabadi, B.; Sircar, J.; Simon, M. E.; Wang, E. N. Design and Modeling of Membrane-Based Evaporative Cooling Devices for Thermal Management of High Heat Fluxes. *IEEE Trans. Compon., Packag., Manuf. Technol.* **2016**, *6* (7), 1056−1065.
(44) Moore, A. L.; Shi, L. Emerging Challenges and Materials for Thermal Management of Electronics. *Mater. Today* **2014**, *17* (4), 163−174.
(45) Spintronics|Annual Review of Condensed Matter Physics. https://www.annualreviews.org/doi/abs/10.1146/annurev-conmatphys-070909-104123 (accessed May 18, 2022).
(46) Žutić, I.; Fabian, J.; Das Sarma, S. Spintronics: Fundamentals and Applications. *Rev. Mod. Phys.* **2004**, *76* (2), 323−410.
(47) An Ab Initio Electronic Transport Database for Inorganic Materials|Scientific Data. https://www.nature.com/articles/sdata201785 (accessed May 18, 2022).
(48) Bansal, D.; Niedziela, J. L.; May, A. F.; Said, A.; Ehlers, G.; Abernathy, D. L.; Huq, A.; Kirkham, M.; Zhou, H.; Delaire, O. Lattice Dynamics and Thermal Transport in Multiferroic $CuCrO_2$. *Phys. Rev. B* **2017**, *95* (5), No. 054306.
(49) Ouyang, Y.; Zhang, Z.; Li, D.; Chen, J.; Zhang, G. Emerging Theory, Materials, and Screening Methods: New Opportunities for Promoting Thermoelectric Performance. *Ann. Phys.* **2019**, *531* (4), No. 1800437.

https://doi.org/10.1021/acsomega.4c01116
ACS Omega 2024, 9, 22831−22838